Planning the Trajectories of Multiple Mobile Sinks in Large-Scale, Time-Sensitive WSNs

Technical Report No. 381/11

Wint Yi Poe, Michael Beck, Jens B. Schmitt

Distributed Computer Systems Lab (DISCO), University of Kaiserslautern, Germany

Abstract. Creating an opportunity from challenges generated by mobility in WSNs prolongs the lifetime of WSNs by relocating the sinks to avoid a hot-spot problem. Such evidence makes a great impact on energy-constrained WSNs. It, however, produces an undesirable information transfer delay. Often the maximum allowable message transfer delay must be bounded in order to enable time-sensitive applications of WSNs, hence, it is crucial to develop a mobile enabled WSNs that minimize the worst-case delay without the loss of a lifetime degradation. To do so, multiple mobile sinks are designed, in particular, for the sink trajectory. In fact, sink trajectory in mobile enabled WSNs is a discrete form of static sink placement in traditional WSNs. In this report, we propose a geometrically principled heuristic for finding good trajectories of multiple mobile sinks in large-scale, time-sensitive WSNs. First, we discuss the high analytical challenges of optimally planning the trajectories of multiple mobile sinks. Based on this, we relax the problem by transforming it into a geometric design problem, which, subsequently, is solved in closed form. The analytical results are compared with Java-based simulation results. The polar grid-based trajectory effectively minimizes the worst-case delay and maximizes the lifetime as, for example in a WSN with 500 nodes and 20 sinks, it has in the order of 50 % lower worst-case delay and 300 % higher lifetime than a random walk trajectory. Hence planning the sink trajectories carefully really pays off.

Keywords. Wireless Sensor Networks, Sink Trajectory, Worst-Case Delay, Lifetime.

1 Introduction

Research activity and application area of wireless sensor networks (WSNs) has been increasing since the last decade. Existing state-of-the-art hardwares and protocols enable testing of the real world applications and provide their substantial research. A deficient energy supply of WSNs drives most of the research towards energy awareness in WSNs. Obviously, energy is a critical issue that is essential in the optimization of the lifetime prolongation of WSNs. In all aspects, such as designs and protocols, numerous energy-aware methods have been proposed and others already defined as the state-of-the-art technology. Among the distinct features of WSNs, a time-sensitive nature is a noticeable problem for application-specific WSNs. The worst-case message transfer delay plays a

vital role in as, for example, intrusion detection application. Therefore, it becomes very interesting to built WSNs such that lifetime and delay goals are met simultaneously.

So, the question is how to design a performance-aware WSN under minimizing the worst-case delay and maximizing the lifetime. In a multi-hop WSN, delay significantly relies on the path length (in hops) from the sources to the sink. Intuitively, the geographic positions of sinks play a vital role in minimizing delay in WSNs. In order to solve the problem of minimizing the worst-case delay, two possible solutions are proposed. One solution is to use a direct communication to the sink by assuming that sensors have enough energy supply. However, because of the limited battery life, this expensive solution is not always feasible in practice, as it results in the loss of coverage. It is only feasible if a sensor is intelligent enough to distinguish the priority of the message. Another solution is to deploy multiple sinks to allow sensors to connect to the nearest sink. By utilizing multiple mobile sinks, the information transfer delay reduces effectively. The latter solution is adequate and preferable for the deficient energy supply of sensor nodes. In order to prolong the lifetime, mobility is a solution. In fact, mobility is a mixed blessing for WSNs. On one hand, the degree of network dynamics induced by mobile nodes or sinks may aggravate the design of networking protocols and distributed algorithms. On the other hand, *controlled mobility* also creates opportunities [10]. One of the successful ways to apply controlled mobility in WSNs is to use a mobile sink in order to avoid the typical hot-spot problem around a static sink [5, 14]. By moving the sink throughout the sensor field, the burden of being a direct neighbor of the sink can be shared among all nodes of the network and the network lifetime increases.

In general, sink mobility as, for example, using random walks of multiple mobile sinks, increases the maximum information transfer delay over that of a proper placement of a set of stationary sinks. This is simply due to the fact that there is always a delay-optimal position for the sink and if the sink is moved away from it the message transfer delay becomes worse. Clearly, this creates a problem for time-sensitive WSN applications. So, using sink mobility, we face a conflict between lifetime maximization and delay bound minimization in large-scale, time sensitive WSNs. The challenge thus becomes to find good trajectories for the sinks such that lifetime and delay goals are met simultaneously. In this report, we first provide a multi-objective optimization problem formulation for planning the trajectories of multiple mobile sinks (called OST (Optimal Sink Trajectory)). We remark that already the single objective problem of maximizing network lifetime is known to be NP-hard [13]. Hence, we relax the OST problem by giving it a geometric interpretation (called GST (Geometric Sink Trajectory)). The intuition behind this is that both, delay and lifetime, benefit from nodes being closer in terms of Euclidean distance to their assigned sinks. So the two objectives are amalgamated into one. Furthermore, the GST lends itself to a solution based on the kernel insight that, for a single sink, the problem is reduced to simply finding a minimum enclosing circle, whose circumcenter is the optimal position for the sink to minimize the maximum Euclidean distance. Extending this insight we propose a geometrically principled approach using a polar grid to divide the sensor field into areas of similar size, each of which is the responsibility of a single sink. The sinks are moved synchronously (e.g., once a day) along an inner and an outer orbit. The optimal size of the inner and outer orbit as well as

the optimal number of sinks on inner and outer orbit are derived in closed form using geometric arguments.

The rest of the report is organized as follows. Section 2 provides an overview of related work. Section 3 describes the network model and, in order to reveal the structure of the problem, provides the original problem formulation for the OST. Next, the GST and its derivations are presented in Section 4. We introduce the MICAz-based energy model in Section 5. The performance of the polar grid-based trajectory for multiple sinks is evaluated and compared against several alternatives using simulations in Section 6. We conclude the report in Section 7.

2 Related Work

Three types of mobile elements have been introduced in WSNs: mobile node, mobile relay, and mobile sinks. The use of mobile nodes can be seen in [4] where the authors introduce the heterogeneous mobile sensors to achieve full coverage. Some related work of mobile relay can be found in [17, 11, 3, 8] where mobile elements act as relays for information gathering. In literature, a number of works rise to the challenge of using multiple mobile sinks [9, 7], yet often not delving into the optimal planning of their trajectories. This section reviews a mobile sink approach and related issues, such as type of sink trajectory and performance issues.

In general, the type of sink trajectory can be categorized as a random, state-dependent, and predefined. The use of the random walk trajectory can be found in [15, 6, 7]. In [7], mobile sinks perform a random walk and collect the data from the sensors of their assigned clusters constructed by load balancing and lifetime maximization. With the random walk trajectory the hot-spot problem is eliminated by distributing the random traffic. It, however, is likely to maximize the worst-case delay in WSNs. Recently, [5, 21] address state-dependent mobility for maximizing the lifetime of WSNs. In their approach, the sink trajectory is a function of a particular network variable, such as, e.g., the state of nodes' batteries; the sink moves either grid-based [5] or following a straight line [21]. Though the lifteime performance of such trajectories is good, the methods assume knowledge of global and dynamic information for determining the optimal paths and sojourn times, which is a very strong assumptions in large-scale WSNs.

The predefined trajectory is fully deterministic where the sink is expected to appear on the same path periodically [9, 11, 22]. In [9], a data collection scheme uses a multi-hop communication for multiple mobile sinks to maximize throughput and to minimize energy consumption. To collect data the mobile sink moves periodically with constant speed along the straight lines. In [11], by fixing the trajectory to be a straight line at the middle of each equal region of the network area (i.e., a rectangular field shape), the authors try to balance the number of sensor nodes for each mobile element services. Intuitively, this model can minimize energy consumption and thus extend the lifetime of WSNs. It, however, does not guarantee a delay optimization. In [22], the authors present a trajectory at the periphery of the network as the best strategy over other fixed trajectories such as mid-periphery, diagonal cross, and mid-cross for load balancing in WSNs, by proving the correctness of [14]. An interesting thing is [20] considered a fixed

trajectory along concentric circles separated by $2r_{tx}$, where r_{tx} is the transmission range of node, for the entire network with the purpose of minimizing total energy consumption. Such trajectory looks similar to our polar grid trajectory but ours is for multiple mobile sinks in which lifetime and delay goals are met simultaneously.

In contrast to a periodical movement, the work in [14] proposes a predefined sink trajectory that appears just one round. Here, the movement of a sink is the sequence of a static sink placement like [23, 15], and the sink velocity and sojourn time are computed according to the expected lifetime of WSNs. At each sojourn along a given trajectory, the sink broadcasts its current location and collects data that are forwarded to it through multi-hop communication. In [15, 14], the improvement of lifetime prolongation by using joint mobility and routing method is presented. In [15], the authors present the problems of determining sink sojourn times at each random sink location and the authors in [14] address a modified periphery sink trajectory with a better routing design that uses a combination of round routes and short paths. Most of these studies are concerned with the lifetime prolongation of a WSN, often restricting to the single mobile sink case.

In our work, we tackle the problem of finding good trajectories for multiple mobile sinks such that we keep the maximum message delay low and still achieve a long lifetime. So, delay and energy are traded off against each other. Along similar lines, [21] optimizes this trade-off, too, designing a trajectory for a "data mule" which collects the data from each sensor node directly [17]. In order to minimize delay, the speed of "data mule" and its improvement, which combines multi-hop communication for those nodes that are far from the sink, are both controlled. Since the "data mule" first collects the data from the root nodes closest to the sink and later transfers all the data to the sink, it is not communicate directly to the sink. Yet, the data mule approach incurs long latencies and is generally not applicable in time-sensitive WSNs. Almost all mobile enabled multi-hop WSNs mentioned above use the shortest path routing except some additional modification in [14, 21].

In [23, 15, 13], the movement of a sink is abstracted as a sequence of a static sink placements assuming that the time scale of sink mobility is much larger than that of data delivery; we follow this assumption in our work. Following similar geometric arguments, [13] focuses on minimizing the *average* distance between sink and assigned sensor nodes. The reasonable assumption is that in a multi-hop network, the energy cost of transmitting a message from the node to the sink is linearly proportional to the Euclidean distance between them. Such a distance-related assumption is also at the heart of our work but with additional consideration of the message transfer delay, which is why we set out to minimize the *maximum* distance.

3 Network Model and Problem Statement

In this section, we first provide our network model along with some basic assumptions and, next, state the problem of planning sink trajectories for multiple mobile sinks as a multi-objective optimization problem. Here, the intention is to shed light on its basic mathematical structure without providing a solution approach yet.

3.1 Network Model

V is the set of sensor nodes with $|V| = N$; S is the set of sinks with $|S| = K$. We model the WSN as a directed graph, $G = (\mathcal{V}, \mathcal{E})$, where $\mathcal{V} = V \cup S$. For all $a, b \in \mathcal{V}$, $\exists (a, b) \in \mathcal{E}$ if and only if a and b are within a disc-based transmission range r_{tx}.

- We assume that the sinks' movement is synchronous, i.e., all sinks move at the same time. Further, sink movement takes places on relatively long time-scales (e.g., once a day), much larger than the time-scale of the message transfer delay from sensors to sinks (e.g., on the order of seconds). Therefore, we neglect the time periods when the sinks are actually moving (or being moved) and the sink mobility is abstracted as a sequence of sinks' locations. At each location the sinks stay for an equal amount of time, further on called epoch $n = 0, 1, 2, \ldots$ In particular, we also assume that all data is flushed from the WSN before a sink movement takes place, i.e., there is no data dependency between epochs.
- The sensor nodes are assumed to be homogeneous: They send $L(n)$ data packets in each epoch n and have the same initial energy budget E available. We focus on the energy consumption for transmitting and receiving data, since the energy consumption by other units is relatively the same for all nodes and, as such, can be taken as a constant. Also, the sensor nodes are stationary.
- We define the locations of sink s in epoch n as $l_s(n) \in \mathbb{R}^2$, and by $l(n) \in \mathbb{R}^{2\times K}$ we denote the sinks' placement in epoch n.
- For node to sink assignment, we define $x_{v,s}(n)$ as a binary variable which is set to 1 if node v is allocated to sink s in epoch n and 0 otherwise. Hence, the overall assignment $X(n)$ in epoch n is a binary matrix:

$$X(n) := (x_{v,s}(n))_{v\in V, s\in S} \in \{0,1\}^{N\times K}.$$

- For a certain assignment $X(n)$ we can define a routing as follows:

$$P_{X(n)} := \bigcup_{v\in V, s\in S\,:\, x_{v,s}(n)=1} P_{v,s}$$

  where, $P_{v,s}$ is a path from node v to sink s which is described as the set of edges lying on this path under the assumption of multi-hop communication.
- We call a sequence of triples

$$\big(l(n), X(n), P_{X(n)}\big)_{\,n\in\mathbb{N}} =: \mathcal{S}_n$$

  a strategy.
- We define the network lifetime by the timespan until the first node dies due to battery depletion.

3.2 Optimal Sink Trajectory: Problem Statement

Based on these definitions, we formulate the optimization problem of finding sink trajectories for multiple sinks in a WSN with the aim of minimizing the

maximum delay and maximizing the network lifetime T of the network:

$$\min_{\mathcal{S}_n} \max_{v \in V,\, n \in \mathbb{N}} D_v(n)$$
$$\max_{\mathcal{S}_n} T$$

subject to: $\forall n \in \mathbb{N}$, $\forall v \in V$, $\forall s \in S$

$$\sum_{e \in \delta^-(v)} f_n(e) - \sum_{e \in \delta^+(v)} f_n(e) = L \tag{1}$$

$$\sum_{e \in \delta^+(s)} f_n(e) = L(n) \sum_{v \in V} x_{v,s}(n) \tag{2}$$

$$\sum_{s \in S} x_{v,s}(n) = 1 \tag{3}$$

$$\sum_{n=0}^{T} \left(\sum_{e \in \delta^-(v)} E_{tx}(e, f_n(e)) + \sum_{e \in \delta^+(v)} E_{rcv}(e, f_n(e)) \right) \leq E \tag{4}$$

where $\delta^-(v) = \{e \in \mathcal{E} | e = (v, n), n \in \mathcal{V}\}$ and $\delta^+(v) = \{e \in \mathcal{E} | e = (n, v), n \in \mathcal{V}\}$. The function $f_n : \mathcal{E} \rightarrow \mathbb{R}^+$ describes the amount of data sent over an edge in epoch n. Equations (1) and (2) are flow balance equations to ensure that no additional data is produced or any data is lost at the nodes. Equation (3) enforces that a sensor node is assigned to exactly one sink in epoch n. The energy constraint for each node $v \in V$ is defined in Equation (4); here, the total energy consumption for reception $E_{rcv}(e, f_n(e))$ and transmission $E_{tx}(e, f_n(e))$ up to epoch T, the lifetime of the WSN, must not exceed the initial energy E for any nodes.

The delay function $D_v(n)$ represents the end-to-end delay characteristics for the message transfer from node v to its assigned sink in epoch n. At this point, we still remain abstract about whether, e.g., an average delay over an epoch or the maximum delay experienced is taken. However, later on (in the simulations as presented in Subsection 6.4), based on sensor network calculus [16], we use a bound on the maximum end-to-end delay to instantiate $D_v(n)$. In any case, the delay function $D_v(n)$ is a very complex function, which does not only depend on the path from the node v to its sink, but also on all other paths interfering with it. Hence, differences in choosing a path for just one node-sink pair, in general, affect multiple end-to-end delays. Similarly, we also remain abstract about the energy functions E_{rcv} and E_{tx}, which are also complex functions, thus aggravating the problem further. A last but not least hardness of the problem stems from the two objective functions and their conflicting nature.

4 Geometric Sink Trajectory (GST)

Due to its fundamental hardness, we relax the OST problem, which is basically a graph problem, into a geometric one, called the Geometric Sink Trajectory (GST) problem. Basing on the assumption of a large-scale WSN with a more or less uniform node distribution we abstract from nodes as such. For the geometric

shape of the sensor field we assume it to be a circle, a somewhat arguable, but often made assumption on this level of abstraction [13]. We briefly come back to a discussion about the circular shape in Section 7.

Under these abstractions for the GST, the objective of minimizing the maximum delay is reduced to the objective of minimizing the maximum Euclidean distance $d_{v,s}(n) = \|l_s(n) - pos(v)\|_2$ from sink $s \in S$ to node $v \in V$ in epoch n; here, $pos(v)$ refers to the position of sensor node v in the Euclidean space. Somewhat more indirectly, we cater for the lifetime maximization by partitioning the sensor field into areas of similar size (per epoch), each of which is under the responsibility of a single sink. The rationale of this being that each sink is roughly assigned a similar number of sensors thus leading towards a good balancing of the forwarding load between areas.

Interestingly, for the single sink case, we remark that by simply substituting the delay function by the Euclidean distance, and neglecting the energy issues, the OST problem becomes a well-known minimum enclosing circle problem [18] (we point out, though, that with K circles the problem remains hard). This problem and its solution by a minimum enclosing circle is illustrated in Figure 1. The center of such a circle is the optimal placement for a sink in terms of minimizing the maximum distance between sink and sensor nodes. We recur to this basic insight several times further on, when we look for optimal positions of sinks in their respective area.

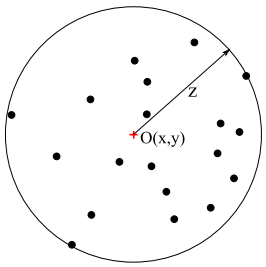

Fig. 1. An example of a minimum enclosing circle.

Our framework to construct sink trajectories $l(n)$ based on solutions to the GST consists of the following steps:

1. We assign areas of similar sizes to the sinks (→lifetime maximization). In fact, there are different possibilities to achieve this and we discuss them in the following subsection.
2. After that we calculate the optimal placement of the sinks, such that the maximal distance of any point in these areas to its sink is minimized (→delay minimization).
3. Finally we define the sink trajectory for each sink by specifying its movement to the next position.

4.1 The Area Assignment Problem

The area assignment problem is: How to partition a circular network of radius R in order to achieve areas of similar size with respect to a given number of sinks K? A first and exact solution is an equal sectorization which has a nice scalability property in terms of handling an increasing number of sinks K without compromising the equal size of each sector. No matter how large K is, equal sectorization achieves equally sized areas by calculating the center angle of each sector as $\Phi = \frac{2\pi}{K}$. Figure 2(a) shows an example of equal sectorization for a 14 sinks network. Due to its symmetrical nature, it is sufficient to find a minimum enclosing circle for one of the circular sectors. Although, the equal sectorization achieves beneficial properties like scalability, congruity, and simplicity, the area of each circular sector becomes increasingly narrower for a growing number of sinks K, which results in relatively large maximum distances to a sink. In fact, the maximum distance for a point to its sink in a circular sector is bounded from below by $\frac{R}{2}$. This implies that the delay performance does not improve significantly any more after a certain number of sinks is reached even if more sinks are available.

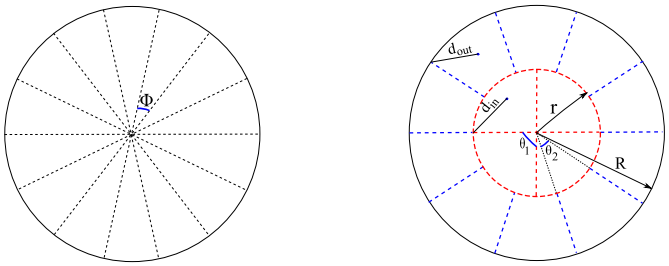

(a) (b)

Fig. 2. Sinks assignment in (a) an equal sectorization, and (b) a polar grid.

Therefore, we introduce an alternative way of partitioning the sensor field, which is designed to improve on minimizing the maximum distance for a growing number of sinks K. The idea is to have two concentric circles of radii r and R, as illustrated in Figure 2(b). By dividing the circle into two different parts, the maximum distance between any point to its sink can be reduced effectively and the resulting scheme still can achieve a balanced area assignment. The resulting partition is usually called a polar grid. The following section describes how to find the optimal sink distribution in a polar grid, i.e., how many of the sinks to place in the outer ring together with the optimal value for the radius of the inner circle r.

4.2 Optimization of the Polar Grid Area Assignment

As shown in Figure 2(b), sinks are assigned in the inner circle and in the annulus of the outer circle to create a polar grid. We define K_{in} and K_{out} as the number of sinks for the inner circle and the annulus of the outer circle, respectively. Figure

2(b) provides an example for 14 sinks with $K_{in} = 4$ and $K_{out} = 10$. Let us define d_{in} and d_{out} as the minimal radii of enclosing circles for the sector and annular segments, respectively, given r, K_{in} and K_{out}. Then, the polar grid-based area assignment problem can be formulated as follows:

$$\min_{0<K_{in}\leq K} \min_{0\leq r\leq R} \max\{d_{in}, d_{out}\} \tag{5}$$

We calculate d_{in} and d_{out} from the corresponding minimum enclosing circles. In the following we assume $K_{in},\ K_{out} \geq 3$ to avoid degenerate cases.

Formulation of d_{in} and d_{out} There are two types of cells in the polar grid-based assignment scheme: a sector in the inner circle and an annular segment in the annulus of the outer circle. The optimal values of K_{in} and K_{out} are likely to be unequal in general, which implies two different center angles θ_1 and θ_2 for sector and annular segment, respectively. This is also illustrated in Figure 3(a) and (b).

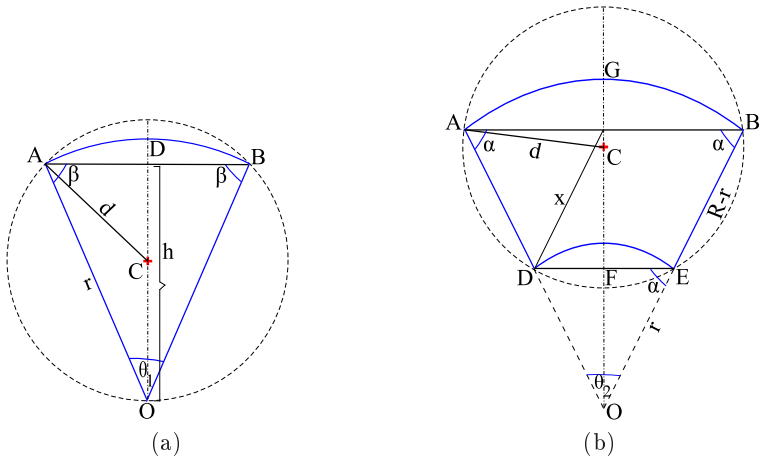

Fig. 3. Circumscribed circles of polar grid cells: (a) a sector in the inner circle, and (b) an annular segment in the annulus.

We find the minimum enclosing circle and its radius by approximating each polar grid cell by an easier shape. In particular, we determine the minimum enclosing circles for the isosceles triangle and isosceles trapezoid for the respective polar grid cells. In Figure 3(a) and (b), the minimum enclosing circles for the isosceles triangle $\triangle ABO$ and the isosceles trapezoid $ABDE$ are depicted, which, in this case, are the circumscribing circles of the triangle and trapezoid, respectively. In the following we denote by h the height in the triangle $\triangle ABO$ and by x the distance between the point E of the trapezoid and the center of the line AB.

The minimal distances d_{in} and d_{out} are calculated from the respective circumscribed circles formulation. Given r, R, α and β (see Figure 3 and 4), the

following equations characterize d_{in} and d_{out}:

$$d_{in} = \begin{cases} \frac{r}{2\sin\beta} & \text{for } \frac{|AB|}{2} \leq h \\ r\cos\beta & \text{for } \frac{|AB|}{2} \geq h \end{cases} \tag{6}$$

$$d_{out} = \begin{cases} \frac{\sqrt{(R-r)^2+4rR\cos^2\alpha}}{2\sin\alpha} & \text{for } \frac{|AB|}{2} \leq x \\ R\cos\alpha & \text{for } \frac{|AB|}{2} \geq x \end{cases} \tag{7}$$

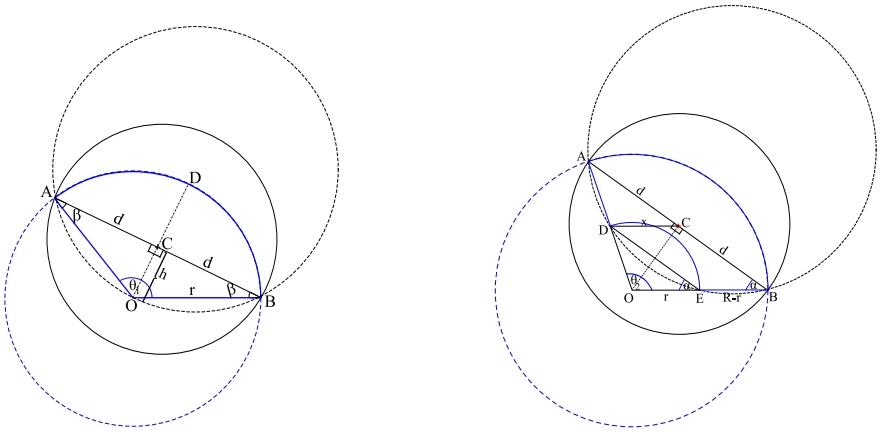

(a) Sector Segment (b) Annular Segment

Fig. 4. Optimal sink placement inside a sector and an annular segment with large $\frac{|AB|}{2}$.

Note that for angles $0 \geq \theta_1, \theta_2 \geq \frac{\pi}{2}$ we always have to consider the first cases of Equations (6) and (7).

The following proofs show the correctness of Equations (6) and (7).

Claim 1: For $\frac{|AB|}{2} \leq h$, the center of the circumscribed circle of the isosceles triangle $\triangle ABO$ minimizes the maximum distance of the sector ABO (refer Figure 3(a)).

Proof: Denote the center of the circumscribing circle by C, its radius by d and the circle itself by C_d. Since $\frac{|AB|}{2} \leq h$ the minimum enclosing circle is C_d. Since $\triangle ABO$ is a subset of the sector, this means that the minimum enclosing circle for the sector has at least radius d. Hence it is sufficient to show that the sector lies inside the circle C_d. Again from $\frac{|AB|}{2} \leq h$ we know that C lies inside the triangle, so $d \leq r$. Obviously $C \neq A, B$ and by this even $d < r$ holds. Denote now by AB_O the arc between A and B with its center in O. It is sufficient to show that any point lying on this arc has distance not bigger than d to C. Denote by D the intersection between the arc AB_O and the line through O and C (see Figure 3(a)). Then by the triangle-inequality (for the triangle $\triangle ACO$) holds:

$$2d \geq r = |OD| = |OC| + |CD| = d + |CD|$$

leading to:

$$d \geq |CD|$$

Suppose now there would exist a point D' on AB_O with $d < |CD'|$. This would only be possible if there exists a point D'' on the arc AB_O which also lies on C_d. Together with A and B this point would be a third intersection point between the circles C_d and O_r, leading to the equality of the two circles, especially to $d = r$, which is a contradiction to the already established inequality $d < r$. Hence all points of the arc, and by this the whole sector, lie inside the circle C_d .

Claim 2: For $\frac{|AB|}{2} \leq x$, the center of the circumscribed circle of the isosceles trapezoid $ABDE$ minimizes the maximum distance of the annular segment $ABDE$ (refer Figure 3(b)).

Proof: As in the previous proof we know, by the assumption that $\frac{|AB|}{2} \leq x$, that the circumscribing circle C_d of the trapezoid is the minimum enclosing circle of the trapezoid and its center lies in the trapezoid. We proceed in the same way as in the previous proof, however here it is not as easy to see that the radius d of the minimum enclosing circle of the trapezoid is smaller than R. For that we denote by F the intersection of the angle bisector of θ_2 with the line $|DE|$ (see Figure 3(b)). The triangle $\triangle AFO$ has its largest angle at F, which is for $r < R$ larger than $\frac{\pi}{2}$ hence:

$$R = |OA| > |AF|$$

A similar argument leads to $|AF| > |DF| = |EF|$, hence we can find an enclosing circle for the trapezoid around F with radius $|AF| < R$ and by this the minimum enclosing circle also has a radius d smaller than R. Now denote again by AB_O the arc between A and B with center in O and by G the intersection between this arc and the line through O and C, where C denotes the center of the minimum enclosing circle. Then again by the triangle inequality:

$$|OC| + |CA| = |OC| + d \geq R = |OC| + |CG|$$

hence:

$$d \geq |CG|$$

By the same contradiction as in the previous proof, one can show that the complete arc AB_O lies inside the minimum enclosing circle of the trapezoid.

Claim 3: For $\frac{|AB|}{2} \geq h$, the line segment AB of the triangle $\triangle ABO$ is the diameter of the minimum enclosing circle (refer Figure 4(a)).

Proof: In the triangle $\triangle ACO$ we have at C a right angle, hence: $d < r$. Denote again by D the intersection of the arc AB_O and the line through O and C, then by the triangle inequality we have:

$$|OD| = |OC| + |CD| \leq |OC| + |CA|$$

Knowing that $|CD| \leq |CA| = d$ we can construct the same contradiction as in the previous proofs to see that the whole arc AB_O lies inside C_d. By this we know that C_d is an enclosing circle. Since $|AB| = 2d$ we also know that any enclosing circle has at least radius d, thus C_d is a minimum enclosing circle.

Claim 4: For $\frac{|AB|}{2} \geq x$, the line segment AB of the trapezoid $ABDE$ is the diameter of the minimum enclosing circle (refer Figure 4(b)).

Proof: The proof works like the previous one replacing r by R and G taking the role of D.

Optimal r and sink distribution K_{in} vs. K_{out} Based on the mathematical formulations for d_{in} and d_{out}, we are able to evaluate expression (5). One sees that for a fixed K_{in} and K_{out} d_{in} is a strictly increasing function in r and d_{out} is a decreasing function in r. So we have to compute the intersection of the two functions d_{in} and d_{out}, which gives us the optimal value for r, given a combination of K_{in} and K_{out}. The global minimum of d_{out} is equal to $R\cos\alpha$ and is achieved at all $r \geq R - 2R\cos^2\alpha$. So to find the intersection of d_{in} and d_{out} we need to know, where the function d_{in} intersects with the function given in the first case of Equation (7). The necessary computations for the case we use the first case of Equation (6) for d_{in} are as follows:

$$\frac{r}{2\sin\beta} = \frac{\sqrt{(R-r)^2 + 4rR\cos^2\alpha}}{2\sin\alpha}$$

$$\Rightarrow \quad r_1, r_2 = \frac{-b \pm \sqrt{b^2 - 4ac}}{2a}$$

where

$$\begin{aligned} a =& \sin^2\alpha - \sin^2\beta, \\ b =& 2R\sin^2\beta(1 - 2\cos^2\alpha), \\ c =& -R^2\sin^2\beta. \end{aligned}$$

By evaluating $\max\{d_{in}, d_{out}\}$ at the minimum of the points $[r_0]_+$, r_1 and r_2 we can find the minimum for this case.

For the case where we use the second case of Equation (6) we proceed similarly:

$$r_1, r_2 = \frac{-e \pm \sqrt{e^2 - 4df}}{2d}$$

$$r_0 = R - 2R\cos^2\alpha,$$

where

$$\begin{aligned} d =& 4\sin^2\alpha\cos^2\beta - 1, \\ e =& 2R - 4R\cos^2\alpha, \\ f =& -R^2. \end{aligned}$$

Again by evaluating $\max\{d_{in}, d_{out}\}$ at the minimum of the points $[r_0]_+$, r_1 and r_2 we can find the minimum of $\max\{d_{in}, d_{out}\}$.

For a given K and R, we can now exhaustively search for the optimal values of r trying all possible combinations of K_{in} and K_{out} (the size of the search space is just $K - 1$). Among all combinations, we select the best configuration of K_{in} and K_{out} with respect to the minimum distance of d_{in} and d_{out} (using the best r), thus implementing Equation (5).

4.3 Designing the Sinks' Trajectories

Now, we know the optimal points (i.e., the centers of the minimum enclosing circles for sector and annular segments) which produce the optimal d_{in} and d_{out}. Based on these points, we design circular mobile sink trajectories. Let r_{in} and r_{out} denote the distances from the center of the network to the center of the minimum enclosing circles for the sector and annular segment, respectively, as illustrated in Figure 5. The formulas for determining r_{in} and r_{out} look like the follows:

$$r_{in} = \begin{cases} \frac{r}{2\sin\beta} & \text{for } 0 \leq \theta_1 \leq \frac{\pi}{2} \\ r\sin\beta & \text{for } \frac{\pi}{2} \leq \theta_1 \leq \pi \end{cases} \tag{8}$$

$$r_{out} = \begin{cases} \sqrt{\frac{(R-r)^2+4rR\cos^2\alpha}{4\sin^2\alpha} - r^2\cos^2\alpha} + r\sin\alpha. & \text{for } r \leq R - 2Rcos^2\alpha \\ R\sin\alpha. & \text{for } r \geq R - 2Rcos^2\alpha \end{cases} \tag{9}$$

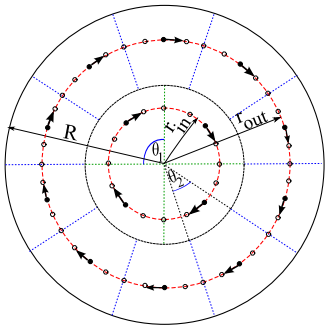

Fig. 5. An example of polar grid_based trajectory for a 14 sinks network.

The trajectories of the sinks basically result from rotating the whole polar grid in an attempt to keep both, message transfer delay and load per sink, balanced. Clearly, an interesting parameter is how far we rotate the polar grid, i.e., which step size we use for each sink when going from one epoch to the other. Results concerning this step size and a deeper discussion of its influence are provided in Section 6.

4.4 Analytical Evaluation of the Geometric Sink Trajectory

Before we delve into a detailed simulative study of our approach, we first analytically compare the equal sectorization and polar grid-based area assignment schemes with each other. Figure 6(a) and (b) show the maximum distance distributions of an equal sectorization- and a polar grid-based area assignment for $R = 100\,m$ and a varying number of sinks K up to 30. Apparently, a polar grid

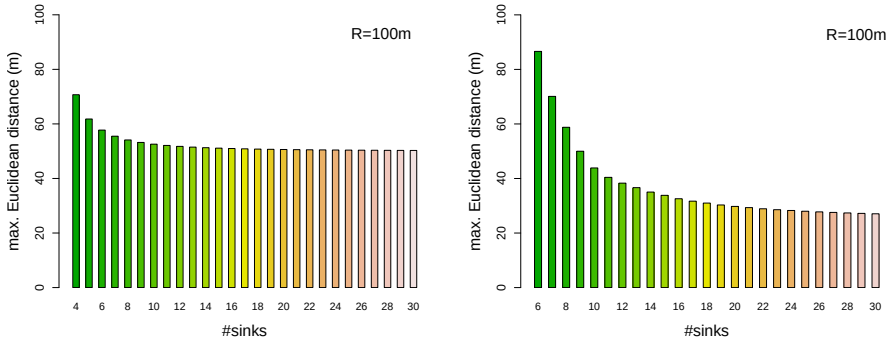

(a) (b)

Fig. 6. The maximum Euclidean distances distribution of (a) an equal sectorization, and (b) a polar grid-based area assignment schemes.

area assignment effectively reduces the maximum distance as K grows. Note that for $K \leq 8$ the equal sectorization is in fact superior to the polar grid. The reason lies in the restriction of having K_{in}, $K_{out} \geq 3$, otherwise the polar grid should always be superior, since equal sectorization can be considered a special case of a polar grid (with $K_{out} = 0$ and $r = R$). The results are based on the optimal choice for r and the optimal sinks distribution for K_{in} and K_{out}.

We further show the corresponding optimal sink distribution K_{in} and K_{out} in Figure 7.

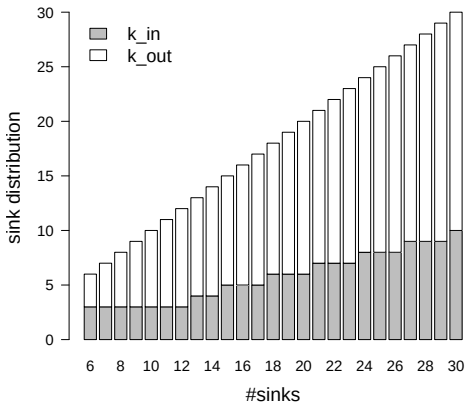

Fig. 7. Optimal sink distributions (K_{in} vs. K_{out}) for the polar grid-based area assignment.

Starting from $K = 13$, the value of K_{in} is $\lfloor \frac{K}{3} \rfloor$ and consequently the value of K_{out} becomes $\lceil \frac{2K}{3} \rceil$. Therefore, the optimal ratio of $\frac{K_{in}}{K_{out}}$ becomes $\frac{1}{2}$. In general, the optimal sink distribution is about one third of the sinks for the inner circle and about two-thirds for the annulus. Furthermore, the calculation shows that the optimal r is converging to half of the radius R.

We remark that, in general, the polar grid does not achieve a perfectly equal area assignment. Nevertheless, the differences are not too large and as discussed in the following section the polar grid performs favorably with respect to both objectives, lifetime maximization and delay minimization.

Accordingly, the optimal r_{in} and r_{out} are shown in Figure 8(a). Figure 8(b) shows the corresponding optimal r distribution for Figure 6(b).

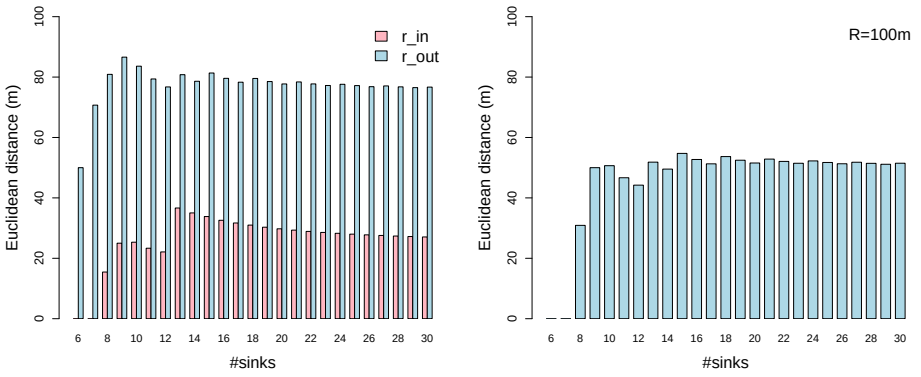

(a) (b)

Fig. 8. (a) An optimal distribution of r_{in} and r_{out}, and (b) The optimal radius r distribution.

5 Energy Model

A sensor node is composed of a sensing unit, a processing unit, a transceiver unit, and a power unit. Each unit consumes a different energy level. Usually, the main consumers of energy are the transceiver unit and the processing unit. The sensing unit consumes energy for a variety of sensors and for ADC converters. The processing unit requires energy to aggregate data, compute routing, and maintain security, etc. Since the purpose of the transceiver unit is to both transmit and receive data, it is no doubt that it consumes quite a lot of energy. If a WSN allows direct communication from a node to a sink, then this will be very expensive. For this reason, we consider multi-hop communication in WSNs, and thus energy consumption by transmitting and receiving a message has to be analyzed based on a hop-by-hop communication scheme.

In fact, a highly accurate energy estimation is desirable. However, this would need to be investigated starting from the transistor level, taking into consideration leakage, etc. We take a more abstract view and define a simple energy model for the assessment and performance comparison of sink trajectory in WSNs.

We make assumptions that the model mainly highlights the energy consumption of the transceiver unit, since the energy consumption of the processing unit is relatively the same for all nodes and, as such, can be taken as a constant. Thus, energy consumption for security, routing, and data aggregation is not taken into account. Wireless signal propagation should be aware of a path loss. Typically, the path loss exponent, τ, varies from 2 to 6. If the environment is a free space, then $\tau = 2$ is considered based on the Friis free space model. Otherwise $\tau = 5to6$ can be considered for shadowed areas and obstructed indoor scenarios [12].

The model concerns total energy consumption of a data packet sent from all nodes to their nearest sinks whenever the sinks move to the next position. As has been mentioned in Subsection 3.1, we define the lifetime of the WSN as the time span until the first sensor node depletes its battery. In order to capture this event we need to keep track of the battery levels of each sensor node. To that end, we define a simple, yet fairly realistic model mimicking the energy consumption of MICAz motes [2]. We focus on the energy consumption of the transceiver unit. The formulation of the total energy consumption for all data transmissions from the nodes to their assigned sinks up to epoch n, is denoted by E^n_{total}; it is the sum of total energy consumption of all nodes:

$$E^n_{total} = \sum_{v \in V} E^n_v \tag{10}$$

where the energy consumption for a node v in epoch n, E^n_v, is given in accordance to Equation (4) as:

$$E^n_v = \sum_{e \in \delta^-(v)} E_{tx}(e, f_n(e)) + \sum_{e \in \delta^+(v)} E_{rcv}(e, f_n(e)),$$

with

$$E_{rcv}(e, f_n(e)) = E_{rcv}(f_n(e)) = P_{rcv} \cdot t_{rcv}(f_n(e)), \tag{11}$$

$$E_{tx}(e, f_n(e)) = P_{tx}(e) \cdot t_{tx}(f_n(e)). \tag{12}$$

In (11), we see that the energy consumption for receiving the data $f_n(e)$ is just the time needed to receive the data $t_{rcv}(f_n(e))$ multiplied by the power consumption P_{rcv} of the receiving unit; this is independent of the distance between the sending and receiving node. In (12), the energy consumption for sending data is again the time needed to send the data $t_{tx}(f_n(e)$ times the power consumption of the sending unit $P_{tx}(e)$, which, however, now is dependent on the distance between the communicating nodes. Taking the values from the MICAz data sheet [2], we can calculate the power consumed by the receiver electronics P_{rcv}. Basically, P_{tx} depends on the transmitted output power setting which again depends on the distance and the selected modulation scheme. There are two components that consume energy in the transmitter part. The formula is

described in Equation (13). The first part represents power used in transmitter electronics, P_{txElec}, while the remaining part is expressed as transmission power of RF signal generation, P_{amp}.

$$P_{tx} = (P_{txElec} + P_{amp}) \tag{13}$$

$$P_{amp} = V \cdot I_{tx} \tag{14}$$

Basically, P_{txElec} can be assumed as a constant, whereas we define P_{amp} in Equation (14). Let us discuss the second component in detail. Although it looks simple, the choice of a current consumption depends on the transmitted output power setting that relies on the distance and the selected modulation scheme. It is impossible to directly use a typical current because with MICAz it does not report a connection between them. Therefore, we must check the relationship (in dB) between RF power, P_{tx}, and the received signal power at distance d, P_d.

We express the transmission model that is based on the specifications of the CC2420 RF transceiver of a MICAz mote [1] using reference [19]. First, we study the effect of a path loss variation over distance between two nodes. The path loss occurs due to the dissipated power at transmitter op-amp and channel propagation. For general analysis of the system design, the transmission power is built upon the mean path loss which is measured in dB, as shown in Equation (15). The mean path loss, $PL(d)$ can be computed using the mean path loss at reference distance d_0, $PL(d_0)$, and the path loss exponent,τ[1].

$$PL(d) = PL(d_0) + 10\tau log_{10}(\frac{d}{d_0}) \tag{15}$$

Based on a free space radio propagation environment, Equation (16) is used to compute the value of $PL(d_0)$.

$$PL(d_0) = 20log_{10}(\frac{4\pi d_0}{\lambda}) \tag{16}$$

where,

$$\lambda = c/f$$

$c := speed\ of\ light$

$f := frequency\ of\ the\ transmitted\ signal.$

We now compute the received signal power at a distance d based on the transmitted signal in dB with the following Equation (17).

$$P(d) = P_{tx} - PL(d) + \sigma \tag{17}$$

Based on the above equation, a distance-dependent corresponding power level for MICAz mote is introduced to check a satisfactory power level for a given distance, d, in [19]. By referring to the Chipcon CC2420 output power setting for the MICAz mote, we get the typical current consumption, and thus P_{amp}.

$$P(d) = \begin{cases} P_{tx} - 40.2 - 20log_{10}(d), & d < 8m \\ P_{tx} - 58.5 - 33log_{10}(\frac{d}{8}), & d > 8m \end{cases} \tag{18}$$

[1] A wide range of $1km$ is considered for cellular system and a short range of $1m$ is considered for WLANs [12].

Note that transmitting uses less energy than receiving even at the highest output power of the transceiver chip. The reason is that the receiver consumes a considerable amount of power due to idling in the receive mode. So, a duty cycle is a good way to control energy consumption of a receiver.

6 Performance Evaluation

In this section, using discrete event simulations, we evaluate the performance of the polar grid-based solution to the GST under the assumptions of the original OST problem formulation. In particular, we compare it to a number of alternative sink trajectories with respect to delay and lifetime performance. Furthermore, we analyze factors like the number of sensor nodes, the number of sinks, and the movement step sizes of the sinks.

6.1 Competitors

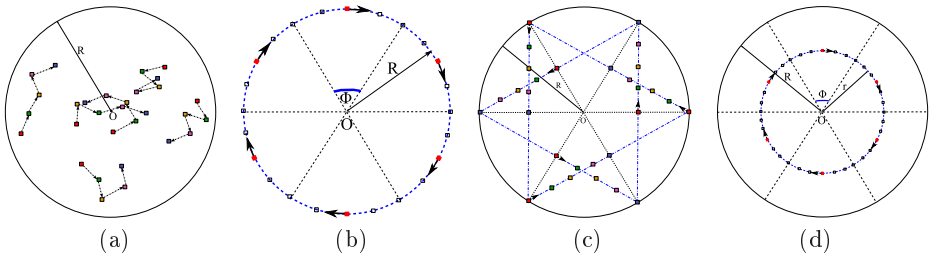

Fig. 9. Competitors: (a) a random walk, (b) an outer periphery, (c) a star, and (d) an equal sectorization trajectory.

We selected four competing sink trajectories which are illustrated in Figure 9(a), (b), (c), and (d). Supposedly as a lower bound among the trajectories, using a random walk (with a fixed step size) for each of initially randomly placed sinks is selected. Clearly, this is a very simple strategy which shall serve as a reference in how far investing more effort in the planning of sink trajectories is justified.

The next competitor is based on an insight by Luo for the single sink case (see Claim 7 in his thesis [13]): using the outer periphery for the sink is actually optimal with respect to lifetime (under mild assumptions about the symmetry of the trajectory). We simply extend this into having multiple sinks circulating in equal distances from each other in the outer periphery.

We construct a star like trajectory as presented in Figure 9 (c). The detail of star trajectory can be seen in the Algorithm 1. In the first step, the network is equally sectorized by the number of sinks. In the second step, we compute λ to decide which vertices are connected to form a star like trajectory. (For example, in a $K = 6$ sinks network, $\lambda = \frac{K}{2} - 1 = \frac{6}{2} - 1 = 2$ then every 2 hops vertices are connected to form a line trajectory.) After that, we initialize the sink for each trajectory. To be able to balance the load and minimize the worst case delay,

Algorithm 1 Constructing a star trajectory.

Given: Number of sinks to be placed $|S| = K$, a circular network C_{OR} field of radius R, step size ω
1. The network is equally sectorized by K
2. Compute λ to decide which vertices are connected for the line trajectory
   if$((K\%2) == 1)$ $\{\lambda = \frac{K}{2}\}$
   else $\{\lambda = \frac{K}{2} - 1\}$
3. Initialize the sinks for the corresponding trajectories
   for all sinks $j \in S$,
    case 1: place sink $s_j = (x_j, y_j)$ at periphery, where $j\%2==0$
    case 2: place sink $s_j = mid\,(s_j, s_{j+\lambda})$ at periphery, where $j\%2==1$
4. Perform the task
5. Compute the next sinks' positions
   for(j=0; j<K; j++) {
    while($s_j \in C_{OR}$) {
     compute $s_j = (x_j, y_j)$ by increasing step size ω along the trajectory
     repeat 4 and 5
    }
    go to 3
   }
6. Repeat 5 until the network dies

some sinks are initialized at the periphery while others are put at the middle of the assigned trajectory.

As a last competitor, Figure 9(d) illustrates an equal sectorization trajectory which, in fact, is constructed exactly as the inner circle of the polar grid-based trajectory mentioned in Figure 5.

Apart from the random walk trajectory, all other trajectories are predefined so that the sinks move along the corresponding trajectory repeatedly until the network dies. We investigate the performance of the polar grid trajectory and other competitors under worst case delay and lifetime.

6.2 Delay Performance

While an average delay analysis is certainly useful for some WSN applications, for time-sensitive WSNs being able to bound the worst-case delay is generally more important. To that end, we evaluate the delay performance of the the different sink trajectories using the framework of sensor network calculus (SNC) [16]. This requires to specify bounds on the arrival and service processes, called arrival and service curves, their actual settings are given in Subsection 6.4.

6.3 Lifetime Performance

The Algorithm 2 shows the evaluation of lifetime for a given sink trajectory with respect to total number of epochs until the first node dies. In our model, each node has the initial energy of E joule and sends a data packet to its nearest sink along the shortest path whenever the sinks move to the next epochs

synchronously. In each epoch, the algorithm keeps track of the battery levels of each sensor node and update the total epochs which has been traversed so far. The algorithm terminates if one of N nodes depletes its energy and returns the lifetime as m epochs.

Algorithm 2 Lifetime evaluation for a given sink trajectory.

Given: Sensor nodes $|V| = N$, sinks $|S| = K$
Initialization: Set initial energy, $e^v_{residual} = E$ for all $v \in V$ and initial epoch $m = 0$
loop: In each epoch, $\forall v, v' \in V$,
while ($e^v_{residual} > 0$ || $e^{v'}_{residual} > 0$) {
1. compute the shortest path $P^m_v = \bigcup_{1 \leq k \leq l} e_k(v, v')$,
$\forall v \in V$, $v' \in V \cup S$, $l :=$#hops in P_v
case 1: $e_k(v, v') = e^v_{tx} + e^{v'}_{rec}$, where $v' \notin S$
case 2: $e_k(v, v') = e^v_{tx}$, where $v' \in S$
2. update $e^v_{residual} -= e^v_{tx}$,
while ($v' \notin S$) {update $e^{v'}_{residual} -= e^{v'}_{rec}$ }
3. update the number of epochs $m++$and go to loop
}
return m

6.4 Results

The primary factors in our simulative experiments are: the number of nodes, the number of sinks, and the step sizes (i.e., the Euclidean distance between two consecutive epochs). In all scenarios, nodes are uniformly distributed over a circular field with radius R. The respective network radii are chosen such that a node density of $\frac{1}{50\,m^2}$ is achieved. A $16\,m$ disc-based transmission range is used. Furthermore, sink assignment is done according to the minimum Euclidean distance between nodes and sinks, whereas shortest path routing is used for path selection. For all experiments, we performed 10 replications for each factor combination and present the average results from these. For the large majority of results, we obtained non-overlapping 95% confidence intervals, so we do not show these in the graphs for reasons of legibility.

For the SNC computations, the popular token-bucket arrival curve and rate-latency service curves are used. In particular, for the service curve we use a rate-latency function that corresponds to a duty cycle of 1 %. For the 1 % duty cycle, it takes $5\,ms$ time on duty with a $500\,ms$ cycle length which results in a latency of $0.495\,s$[2]. The corresponding forwarding rate becomes $2500\,bps$.

For the lifetime evaluation, the nodes are set to an initial battery level of $0.1\,joule$. The packet size is assumed to be 100 bytes. Based on $\tau = 2$ for the free space propagation, we apply Equation (18) in order to get the current consumption. In all scenarios a packet transmission incurs a current consumption of $8.5\,mA$ with$-25\,dBm$ for distances up to $12.5\,m$, and $9.9\,mA$ for distances

[2] The values are calculated based on the TinyOS files CC2420AckLpl.h and CC2420AckLplP.nc.

between $12.5\,m$ and $23\,m$ with $-20\,dBm$. Here, a transmission data rate of $250\,Kbps$ is used, which takes $t_{tx} = 3.2\,ms$ for a $100\,byte$ packet. A constant voltage of $3\,V$ is used to transmit and receive modes. We use a current of $19.7\,mA$ for the consumed power by the receiver electronics with a $1\,\%$ duty cycle for receiving a data packet. With these assumptions, we apply Equations (10) to (18).

Experiment 1: Varying the number of nodes and sinks under a fixed step size The simulation results of the worst-case delay for the different competitors over 20 epochs are shown in Figure 10(a) and (b) for a 200-nodes-10-sinks and 500-nodes-20-sinks WSN, respectively. Here, the step size of the equal sectorization trajectory resulting from a movement by a center angle of 10 degrees is used as a reference for the step sizes in the polar grid, outer periphery, star, and random walk trajectories.

In both scenarios, the polar grid trajectory achieves significantly lower worst-case delays than its competitors (especially in the 500 node network). On average, the polar grid achieves about $50\,\%$ lower delays than the random walk and the outer periphery and roughly $20\,\%$ lower delay than the equal sectorization and the star. As we expected, the random walk trajectory provides a high worst-case delay. At first glance surprisingly, the outer periphery performed even worse than the random walk, though, due to the fact that the sinks are rather far away from some of the nodes this is not unreasonable. The star trajectory produces a better delay bound than the equal sectorization for the growing amount of nodes and sinks. An interesting thing is the star trajectory can compete the polar grid at some epochs of the trajectory. The equal sectorization produces fairly good delays in the smaller network but cannot stay close to the polar grid in the larger one. So we validated its lesser scalability in terms of delay performance as it was already indicated in the analytical evaluation in Subsection 4.4.

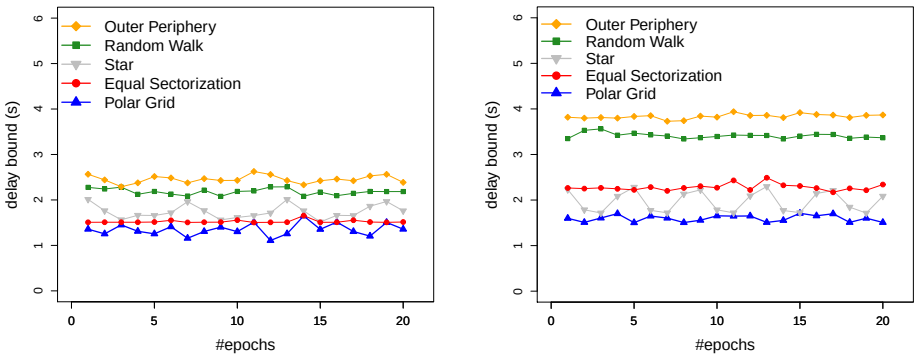

(a) (b)

Fig. 10. The worst-case delay comparisons of (a) 200 nodes with 10 sinks network, and (b) 500 nodes with 20 sinks network.

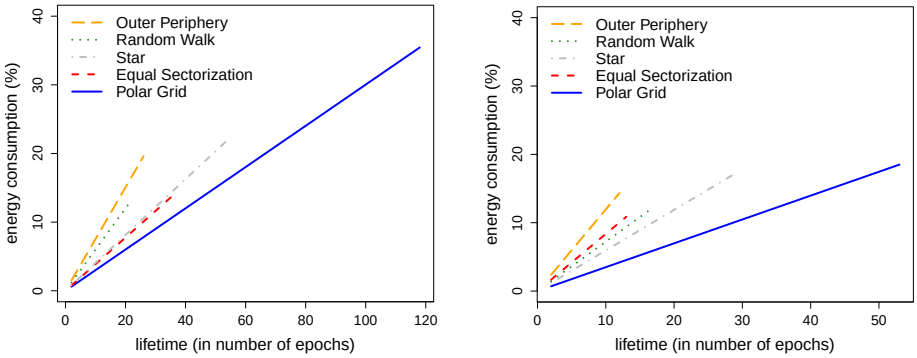

(a) (b)

Fig. 11. The lifetime comparisons of (a) 200 nodes with 10 sinks network, and (b) 500 nodes with 20 sinks network.

The results for the lifetimes of the five competitors are shown in Figure 11(a) and (b). Here, the x-axis represents the lifetime of the WSN (in number of epochs). The y-axis indicates the percentage of the total energy consumption of the whole network during the lifetime of the WSN. As can be observed, the polar grid trajectory strongly outperforms the other trajectories in both scenarios. On average, the polar grid achieves a 440 %, 450 %, 100 %, and 330 % higher lifetime than the random walk, outer periphery, star, and equal sectorization trajectories, respectively. From Figure 11 it becomes clear that this is mainly for two reasons: (1) it requires less total energy per epoch and (2) it drains the energy from the sensor field in a more balanced fashion (indicated by having a higher total energy consumption when the network dies). We can see such effects in the star trajectory although it achieves 50 % lifetime of the polar grid trajectory. It may be noteworthy that the equal sectorization actually performs worse than the random walk in the 500 node network indicating that it does not scale well with respect to lifetime due to a high energy consumption per epoch as well as not being successful in avoiding hot-spot problems. Similarly, the outer periphery performs worse than the random walk in the 500 node network. This is even a bit more surprising than its inferior delay performance, as single sink outer periphery trajectory maximizes lifetime. So, this indicates that the multiple sinks trajectory problem is quite different from its single sink counterpart.

Experiment 2: Varying sinks under the same network In the next experiment, the effect of the number of sinks for each of the competitors is evaluated. Apart from varying the number of sinks, we use the same settings as for Experiment 1. Figure 12 provides the results for the delay bounds under different number of sinks in a 500 node network. As can be seen, the trajectories that are really able to exploit a growing number of sinks to reduce the delay significantly are the polar grid and the star; the outer periphery and the equal sectorization are actually quite insensitive to it, the random walk exhibits a rather chaotic

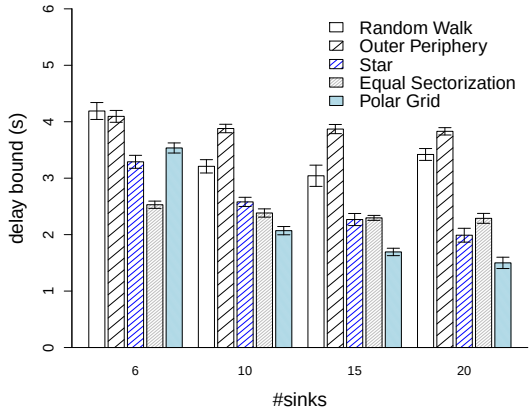

Fig. 12. Delay bound comparison under different numbers of sinks in a 500 node network.

behavior (20 sinks are worse than 10 sinks). You may note that in the 6 sinks case the equal sectorization outperforms the polar grid. In this scenario, the star trajectory is even better than polar grid trajectory. For the growing amount of sinks, the delay bounds of equal sectorization trajectory do not differ too much and the polar grid is significantly better than others. This, as already discussed in Subsection 4.4, is due to the artefact that $K_{in}, K_{out} \geq 3$ disables an effective optimization of the polar grid trajectory for this small number of sinks. In a certain sense it shows that an unoptimized polar grid can also perform unfavorably.

Experiment 3: Varying step sizes under the same network From Experiment 1 and 2, we can clearly see that the polar grid trajectory is a promising heuristic for minimizing the worst-case delay and maximizing the lifetime of large-scale WSNs. In this last experiment, we now investigate the effect of varying the step size of the polar grid trajectory. For this, we focus on the lifetime performance for different step sizes as the delay performance is not particularly sensitive to these. Figure 13(a) and (b) show the lifetimes of the polar grid trajectory for different step sizes in a 200 node network with 10 sinks (here (b) provides a zoom-in for an interesting range of (a)). The corresponding total energy consumption of Figure 13(a) is presented in Figure13(c). The interpretation of the x-axis for Figure 13(a) and (c) is as follows: based on the center angle of an annular segment $\theta_2 = \frac{2\pi}{K_{out}}$, the different step sizes are computed as $\frac{\theta_2}{n}$, where n represents the value of the x-axis; this means the x-axis runs from large step sizes to very small ones. More specifically, the optimal value of K_{out} in this experiment is 7 (out of 10 sinks) and thus $\theta_2 = \frac{2\pi}{7}$ and the step size is varied by letting $n = 2^k$ for $k = 0, ..., 9$.

From this experiment, we can see that the step size has a significant effect in prolonging the lifetime. In particular, it is neither good to move too much or too little, but there is a step size that optimizes the lifetime. For comparison, we also show the performance of a static polar grid-based sink placement, which basically provides the baseline lifetime performance. Hence, this shows another time that sinks mobility pays off, but most if the trajectory is designed carefully (in fact, random walk and equal sectorization performed worse than the static polar grid). A zoom-in for the interesting range of n between 8 and 32, where the optimum step size lies for this experiment, is shown in Figure 13(b). As can be observed, the lifetime behavior is rather chaotic in this range, which hints at the difficulty of obtaining a closed form for the optimal step size under the polar grid, which we leave for future work.

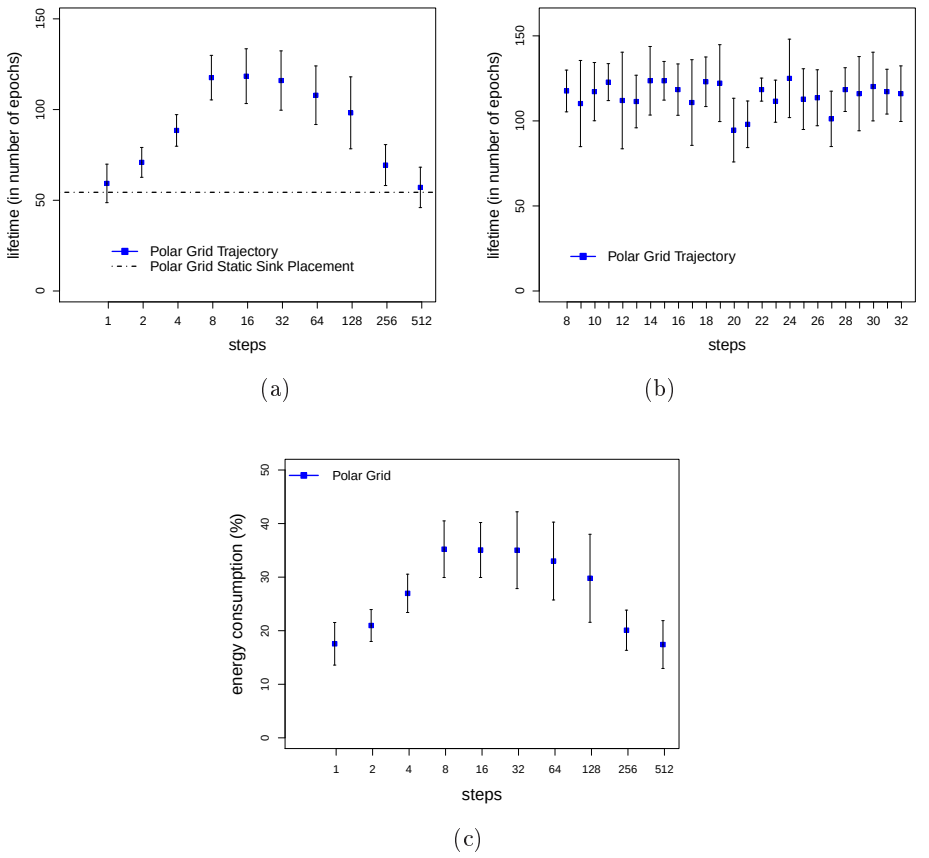

Fig. 13. Lifetime comparisons under varying step sizes in a 200 nodes with 10 sinks network.

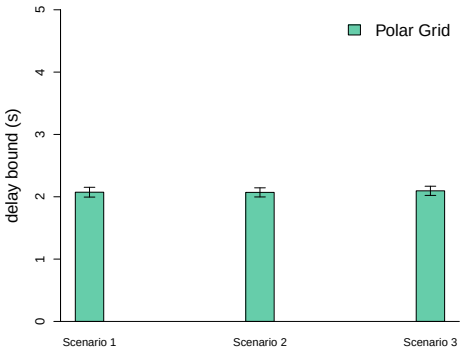

Fig. 14. Delay bounds under three scenarios of different step sizes in 500 nodes with 10 sinks network.

Varying step size does not differ too much for the issue of minimizing the maximum delay as presented in Figure 14. The figure shows the delay bound of 500 nodes with 10 sinks network under three scenarios: (1) step size equivalent to the center angle 5 degree, (2) step size equivalent to the center angle 12 degree, and (3) step size equivalent to the center angle 16 degree. As shown in Figure 14, the delay performance is not sensitive under varying step size and the result remains the same for too much or too little step sizes.

7 Conclusion

In this report, we addressed the problem of finding good trajectories for multiple mobile sinks in WSNs with respect to both, minimizing worst-case delay and maximizing the lifetime of the network. Due to its fundamental hardness, we resorted to a geometric interpretation of the problem for which we introduced and optimized a polar grid trajectory. The simulation results exhibited a very promising delay and lifetime performance for the polar grid trajectory when compared to other trajectories.

As the design space for possible sink trajectories is huge it is tempting to contemplate a bit about extensions as well alternatives to the polar grid trajectory. An obvious extension of the two orbit model used by our polar grid is to use n orbits. Going to n orbits, however, will be harder to optimize by enumeration as the search space for distributing K sinks over n orbits grows as $\binom{K-n-1}{n-1}$ (allowing orbits to be empty). Apart from applying heuristics for that search, one could strive for a closed-form expression over the maximal distances in the n-orbit polar grid to avoid this combinatorial explosion. While this seems hard it would constitute an important step in the general understanding of concentric trajectories.

Non-concentric, but still periodic (following a closed circuit) strategies are imaginable, for example a star shaped trajectory. As a generalization of the concentric class of strategies one may hope for further improvement under the assumption of a successful optimization. In fact, we have experimented with a specific (unoptimized) star-shaped trajectory, yet it was inferior to the polar grid trajectory.

Even for non-periodic trajectories, like the random walk, one may see a case if suitably enhanced. For example, a biased random walk which tries to avoid areas of low energy could perform well with respect to lifetime maximization, though this involves a certain state-dependence which may be undesirable in large-scale WSNs.

At last, we briefly want to discuss how to possibly relax certain assumptions we made throughout the report leading to further future work items. Dispensing with the assumption of a circular field could certainly be interesting. One direct way may be to go for an ellipsoid shape, which would probably still allow for a similar approach to the one presented in this report, based on a suitably generalized polar grid (probably with segments of unequal size within one orbit). Similarly, we have made assumptions on node homogeneity and uniform distribution of nodes. Both of these may be relaxed by going to a three-dimensional geometric interpretation of the original problem where the third dimension could capture, e.g., nodes with (initially) higher battery levels or areas of higher node density. Clearly, the problem will not become simpler, but based on the good experience we made with the geometric interpretation of the underlying problem, we believe that this could be a winning strategy also for such advanced problem settings.

References

1. Chipcon cc2420 datasheet: 2.4 ghz ieee 802.15.4/ zigbee-ready rf transceiver.
2. Crossbow technology inc. mpr-mib users mannual, June 2007.
3. Waleed Alsalih, Selim G. Akl, and Hossam S. Hassanein. Placement of multiple mobile data collectors in underwater acoustic sensor networks. In *ICC*, pages 2113–2118, Beijing, China, 2008. IEEE.
4. N. Bartolini, T. Calamoneri, T. L. Porta, A. Massini, and S. Silvestri. Autonomous deployment of heterogeneous mobile sensors. In *ICNP*, pages 42–51, 2009.
5. Stefano Basagni, Alessio Carosi, Emanuel Melachrinoudis, Chiara Petrioli, and Z. Maria Wang. Controlled sink mobility for prolonging wireless sensor networks lifetime. *Wireless Sensor Network, Springer Netherlands*, 14(6):831–858, December 2008.
6. Ioannis Chatzigiannakis, Athanasios Kinalis, and Sotiris Nikoletseas. Sink mobility protocols for data collection in wireless sensor networks. In *Proceedings of the 4th ACM international workshop on Mobility management and wireless access, MobiWac*, volume 44, pages 52–59, New York, NY, USA, October 2006. ACM.
7. Ioannis Chatzigiannakis, Athanasios Kinalis, Sotiris Nikoletseas, and Jose Rolim. Fast and energy efficient sensor data collection by multiple mobile sinks. In *Proceedings of the 5th ACM international workshop on Mobility management and wireless access*, MobiWac '07, pages 25–32, New York, NY, USA, 2007. ACM.
8. C. Chen, J. Ma, and K. Yu. Designing Energy-Efficient Wireless Sensor Networks with Mobile Sinks. In *Proceeding of the 4th ACM Conference on Embedded Networked Sensor Systems (SenSys 2006)*, Boulder, Colorado, USA., October 2006.

9. Shuai Gao, Hongke Zhang, and Sajal Das. Efficient data collection in wireless sensor networks with path-constrained mobile sinks. In *IEEE International Symposium on a World of Wireless, Mobile and Multimedia Networks and Workshops, WoWMoM*, October 2009.
10. David K. Goldenberg, Jie Lin, A. Stephen Morse, Brad E. Rosen, and Y. Richard Yang. Towards mobility as a network control primitive. In *Proceedings of the 5th ACM international symposium on Mobile ad hoc networking and computing, MobiHoc*, pages 163–174. ACM Press, 2004.
11. David Jea, Arun Somasundara, and Mani Srivastava. Multiple controlled mobile elements (data mules) for data collection in sensor networks. In *Lecture Notes in Computer Science*, pages 244–257. Springer, 2005.
12. H. Karl and A. Wittig. *Protocols and Architectures for Wireless Sensor Networks.* Wiley, 2005.
13. Jun Luo. *Mobility in Wireless Networks: Friend or Foe - Network Design and Control in the Age of Mobile Computing.* PhD thesis, School of Computer and Communication Sciences, EPFL, Switzerland, 2006.
14. Jun Luo and Jean-Pierre Hubaux. Joint mobility and routing for lifetime elongation in wireless sensor networks. In *Proceeding of the 24th Annual Conference of the IEEE Communications Societies (INFOCOM)*, March 2005.
15. I. Papadimitriou and L. Georgiadis. Maximum lifetime routing to mobile sink in wireless sensor networks. In *Proceedings of the International Conference on Software, Telecommunications and Computer Networks, SoftCOM*, September 2005.
16. J. B. Schmitt and U. Roedig. Sensor Network Calculus - A Framework for Worst Case Analysis. In *Proceedings of the International Conference on Distributed Computing in Sensor System (DCOSS05)*, June 2005.
17. Rahul C. Shah, Sumit Roy, Sushant Jain, and Waylon Brunette. Data mules: Modeling a three-tier architecture for sparse sensor networks. In *IEEE Workshop on Sensor Network Protocols and Applications (SNPA)*, pages 30–41, 2003.
18. Michael Ian Shamos and Dan Hoey. Closest-point problems. *16th Annual Symposium on Foundations of Computer Science, FOCS*, pages 151–162, 1975.
19. R. Shokri, P. Papadimitratos, M. Poturalski, and J. P. Hubaux. A Low-Cost Method to Thwart Relay Attacks in Wireless Sensor Networks. Project Report IC-71, Security and Cooperation in Wireless Networks, Doctoral School of the I and C School of EPFL, 2007.
20. Arun A. Somasundara, Aman Kansal, David D. Jea, Deborah Estrin, and Mani B. Srivastava. Controllably mobile infrastructure for low energy embedded networks. *IEEE Transactions on Mobile Computing*, 5:958–973, 2006.
21. Ryo Sugihara and Rajesh K. Gupta. Optimizing energy-latency trade-off in sensor networks with controlled mobility. In *28th IEEE International Conference on Computer Communications, Joint Conference of the IEEE Computer and Communications Societies, INFOCOM*, pages 2566–2570, Rio de Janeiro, Brazil, April 2009.
22. Natalija Vlajic and Dusan Stevanovic. Sink mobility in wireless sensor networks: a (mis)match between theory and practice. In *Proceedings of the International Conference on Wireless Communications and Mobile Computing: Connecting the World Wirelessly, IWCMC*, pages 386–393, Leipzig, Germany, June 2009.
23. Z. Maria Wang, Stefano Basagni, Emanuel Melachrinoudis, and Chiara Petrioli. Exploiting sink mobility for maximizing sensor networks lifetime. In *Proceeding of the 38th Hawaii International Conference on System Sciences*, Big Island, Hawaii, January 2005.